Orientation-Dependent Visibility of Long Thin Objects in Polarization-Based Microscopy

Rieko Arimoto* and John M. Murray‡
*Marine Biological Laboratory, Woods Hole, Massachusetts 02543, and ‡Department of Cell and Developmental Biology, University of Pennsylvania School of Medicine, Philadelphia, Pennsylvania 19104-6058 USA

ABSTRACT Under conditions of directional illumination, the visibility of long, thin objects depends very strongly on the direction and polarization of the incident light. Solutions to Maxwell's equations for the case of an infinite cylinder in an electromagnetic field are well known, and have been used by others in the past for theoretical analysis of light scattering by long, thin objects. The existence of those solutions allows us to calculate the expected angular distribution and polarization of the light scattered from long, thin objects illuminated by a plane wave at any angle. In this paper we show for the first time how one can incorporate these solutions of Maxwell's equations into a quantitative description of the expected appearance of filamentous biological structures in polarization-based microscopy. Our calculations for unidirectional polarized illumination show that thin, dielectric linear objects such as microtubules (or shallow interfaces) observed with finite aperture optics 1) are totally invisible when the angle (ϕ) between the object's long axis and incident illumination is outside the range $|90 - \phi| \leq \sin^{-1}[1.33/\text{N.A.}_{obj}]$ degrees; and 2) are seen with maximum intensity when $\phi = 90°$ for incident illumination and scattered light polarized, either both parallel or both perpendicular to the long axis of the object; whereas 3) two maxima appear at $\phi \cong 90 \pm 25°$ for polarization of the incident illumination parallel to, but the scattered light perpendicular to the long axis, or vice versa; and 4) in either of these latter conditions, the objects are invisible when the illumination is near normal incidence. These counterintuitive predictions were exactly borne out by our experimental measurements of light-scattering intensity from flagellar axonemes as a function of orientation in a polarizing microscope. These calculations and measurements provide a foundation for furthering our understanding of textural or form birefringence. Calculations based on a solid cylinder model accurately predict the shapes of the measured intensity versus orientation curves. However, the relative intensities of axonemes viewed with different polarizer-analyzer settings differ from those calculated for a homogeneous solid cylinder. Thus we find that these relative intensities can provide a sensitive probe for the structure of biological objects with diameters much smaller than the wavelength of light.

INTRODUCTION

Light scattering is the basis for visualizing very small biological objects that are otherwise difficult to see in the microscope. In a previous paper, a form of dark-field microscopy was used to observe microtubules gliding on a glass surface. Surprisingly, although individual microtubules were bright and easily visible, it was found that only a small fraction of the microtubules present were actually being seen (Murray and Eshel, 1992). The visible microtubules were all parallel to each other. In other words, under the conditions of those observations, the visibility of the microtubules depended strongly on their orientation. A partial explanation of this orientation dependence was proposed, but no quantitative comparison between the observation and the explanation was attempted (Murray and Eshel, 1992). More recently, we found that the explanation proposed in the earlier study did not in fact account accurately for the observed dramatic dependence of light scattering upon orientation. This discrepancy between theory and experiment provided the initial motivation for starting the more extensive work reported here.

The basic observation is that under some conditions, long, thin objects such as microtubules or flagella can be brightly visible in a microscope, but then suddenly disappear from view if their orientation with respect to the direction of illumination changes by a very small amount, even just a few degrees. We began the present experiments with the idea that, while this is a fascinating and counterintuitive phenomenon, it is rather arcane and is restricted to certain special conditions unlikely to be encountered in routine microscopy. However, to our surprise, a deeper understanding of what we were observing brought with it the realization that these same effects must be present in all forms of microscopy, and that they are potentially a source of artifacts in any form of microscopy that utilizes polarized light. Furthermore, we find that some aspects of the light scattering reveal structural details of the specimen that are much smaller than the wavelength of light. We present here a first approximation to the quantitative description of images of elongated objects as observed in a polarizing microscope with unidirectional illumination with a collimated beam of light, but which has finite N.A. (numerical aperture) for observation. In a second report we will extend this treatment to ordinary microscopic conditions with finite N.A. for both the illuminating and observing optics.

Received for publication 24 January 1996 and in final form 14 March 1996.

Address reprint requests to John M. Murray, Department of Cell and Developmental Biology, University of Pennsylvania School of Medicine, Philadelphia, PA 19104-6058. E-mail: murray@anat3d1.anatomy.upenn.edu.

Rieko Arimoto's present address is Research and Development Department, Nikon Co., 1-6-3, Nishi-ohi, Shinagawa-ku, Tokyo 140, Japan.

0006-3495/96/06/2969/12 $2.00

MATERIALS AND METHODS

Sample preparations

Axonemes were prepared from sea urchin (*Strongylocentrotus purpuratus*) sperm flagella by shearing and demembranation as described by Gibbons (1982). Twenty microliters of the axoneme suspension in 10 mM Tris-Cl, 2 mM $MgSO_4$, 0.2 mM EDTA, 2 mM EGTA (pH 8.0) was placed on a 24 × 50 mm no. 2 (0.21 mm thickness) coverslip, allowed to adhere to this surface for a moment, and then covered with an 18 × 18 mm no. 11/2 (0.17-mm thickness) coverslip. The edges of the thin coverslip were sealed with clear nail polish to prevent evaporation.

Microscope and illumination system

For illuminating the specimen, we generated an evanescent wave at the interface between the glass coverslip and the aqueous sample buffer. We replaced the microscope condenser with a 2.5-cm cube of BK-7 glass. One edge of the cube (see Fig. 1) was attached with silicone rubber cement to a dual-axis goniometer (Melles-Griot). The holder for the glass cube was designed so that its bottom face was centered at the intersection of the axes of rotation of the two goniometers, thus allowing tilt about either axis with no translation. The goniometer–glass cube assembly was attached by a spacer arm to a three-axis micro-positioner mounted on the rear post of a Nikon Diaphot 300 inverted microscope. The goniometers were used to make the bottom surface of the cube exactly perpendicular to the optic axis. The micro-positioner served to align the center of the bottom face on the optic axis and to lower the cube until it made contact with a droplet of immersion oil placed on the specimen coverslip.

Light from a 100-W high-pressure mercury arc lamp was passed through a green (546 nm) interference filter and formed into a narrow, approximately collimated beam by using the focusing lens of the Nikon lamp housing and a 2-mm aperture positioned 10 cm in front of the lamp. This beam was directed at the side of the glass cube with two steering mirrors, and vertically or horizontally polarized with a sheet of Polaroid film positioned between the last mirror and the cube (see Fig. 1). The angle of incidence on the side of the cube was arranged to be less than 45°, which ensured that the light was totally internally reflected at the specimen coverslip–water interface. After being totally reflected, most of the light exited the side of the cube opposite the entry site, but a small fraction, expected to be approximately 4%, was reflected back into the cube at this glass-air interface. We chose the dimensions of the cube and its location relative to the optic axis so that the secondary reflections of this beam did not bring it back into the field of view of the microscope's objective lens.

For some experiments, a 25-mW air-cooled argon ion laser was used as the light source. In this case the beam from the laser was directed into the steering mirrors as above, with no intervening lenses or apertures.

Data collection and analysis

The specimen was attached to a rotating stage that could be positioned with a precision of approximately 1°. Images of the sample rotated to various orientations were observed through a 40× NA 0.8–1.4 objective lens with iris diaphragm. Images were recorded with a Dage C72 video-rate charge-coupled device (CCD) camera and captured in TIFF format by using a Scion LG3 board in a Macintosh Quadra 700 computer and NIH Image software. The manual gain and black level controls and on-chip integration

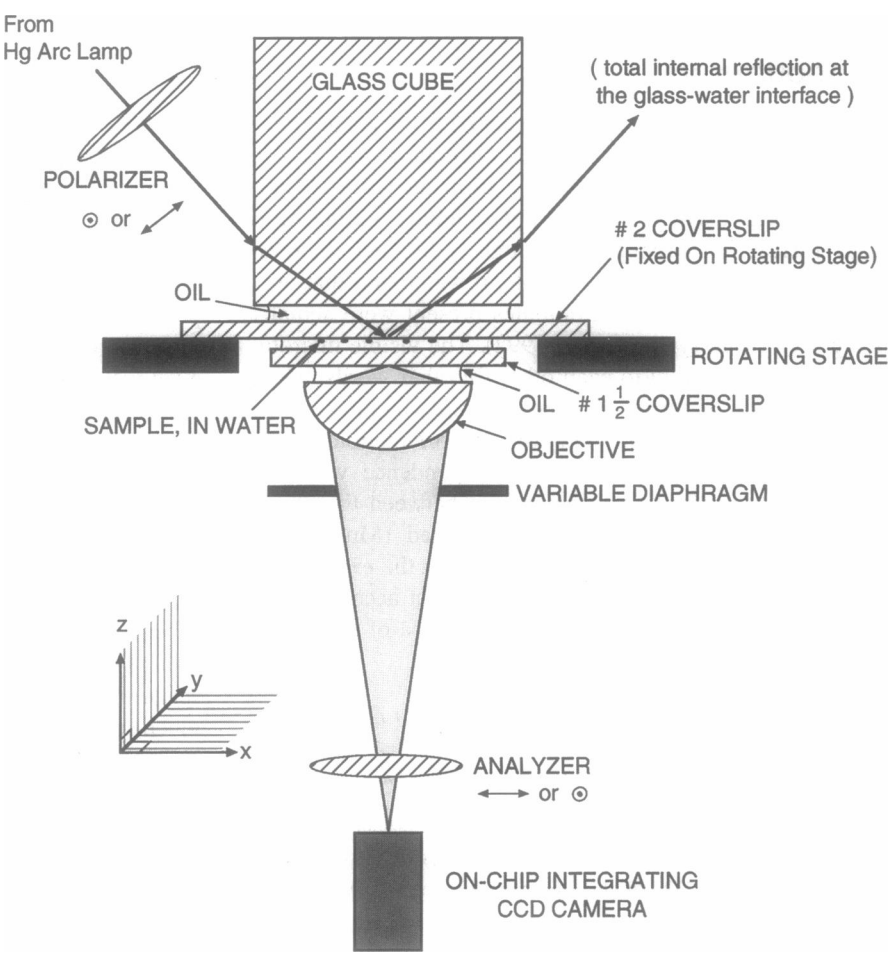

FIGURE 1 Experimental setup. Schematic illustration of the apparatus used for measuring light scattering as a function of illumination angle. Light from a mercury arc lamp was passed through a green interference filter and formed into a narrow, approximately collimated beam. This beam was directed at the side of a glass cube by using steering mirrors, and polarized by using a sheet of Polaroid film positioned between the last mirror and the cube. The angle of incidence on the side of the cube was arranged to be less than 45°, which ensured that the light was totally internally reflected at the specimen coverslip-water interface. The coordinate system used for describing the polarization of the evanescent wave is indicated on the left. A suspension of flagellar axonemes was mounted between two coverslips. The larger coverslip was attached to a rotating stage that could be positioned with a precision of ~1°. The upper coverslip was optically coupled to the glass cube with a thin layer of oil with matched refractive index. A drop of immersion oil coupled the lower coverslip to the objective lens. Images of the sample rotated through the complete range of observable orientations in 4° increments were observed through a 40× NA 0.8–1.4 objective lens with iris diaphragm. Images were recorded with a Dage C72 CCD camera

time were chosen so that images in a series could be recorded in an 8-bit dynamic range with no zeros and no overflow pixels. Thus, because the photometric response of the CCD is precisely linear, differences in pixel intensity in our recorded images are a quantitative measure of differences in light scattered from the specimen. NIH Image was used to measure the background corrected integrated intensity of axonemes in the field of view, and to determine the angle between their long axis and the direction of illumination. To measure the axoneme intensity, we drew a box around each axoneme, summed the intensities of all the pixels in the box, then subtracted [size of box × local background intensity] from the sum.

Theoretical calculations

All calculations were performed using Mathematica (Wolfram Research, Inc.). The starting point for the calculations was the analysis given by Bohren and Huffman (1983) for light scattering by infinite homogeneous cylinders, with TM and TE mode illumination, as a function of illumination angle (ϕ), observation angle (θ), and distance (r). The equations derived in that work were used to calculate three tables of scattered amplitude (see Results and Fig. 2 for definitions of the variables). Each table contained the complex amplitude of the scattered light for a single mode of scattering (i.e., one combination of incident light and scattered light polarizations; E_{11}, E_{22}, or $E_{12} = E_{21}$) over the observable ranges ($90° \pm \sin^{-1}$ [N.A./1.33]) of ϕ and θ in increments of 1°. Each entry of a table gives the complex amplitude of scattered light at a fixed distance from a cylinder (approximately the distance to the entrance aperture of the objective lens) for a single combination of ϕ, θ, and state of polarization. Three factors act to prevent the microscope's camera from receiving all of this light. First, an angle- and polarization-dependent fraction of the light is reflected at the water-coverslip interface and never enters the objective lens. Second, we are observing the scattering through a lens of finite aperture, and the imperfect contrast transfer function of the microscope means that high-angle light is transmitted less efficiently than low-angle light. Third, we placed a polarizing filter en route to the camera, thus allowing only one polarization component to pass for each measurement.

To calculate the expected image intensity for a particular orientation of the specimen, we numerically integrated the rows of the three tables (i.e., constant ϕ values), weighting each entry before integration by the three factors listed above, and then squared the modulus of the result. In an 80-MHz Power Macintosh 7100, the calculation of the three tables required about 2 h, and the numerical integration plus weighting required approximately 30 min for the entire observable range of illumination angles.

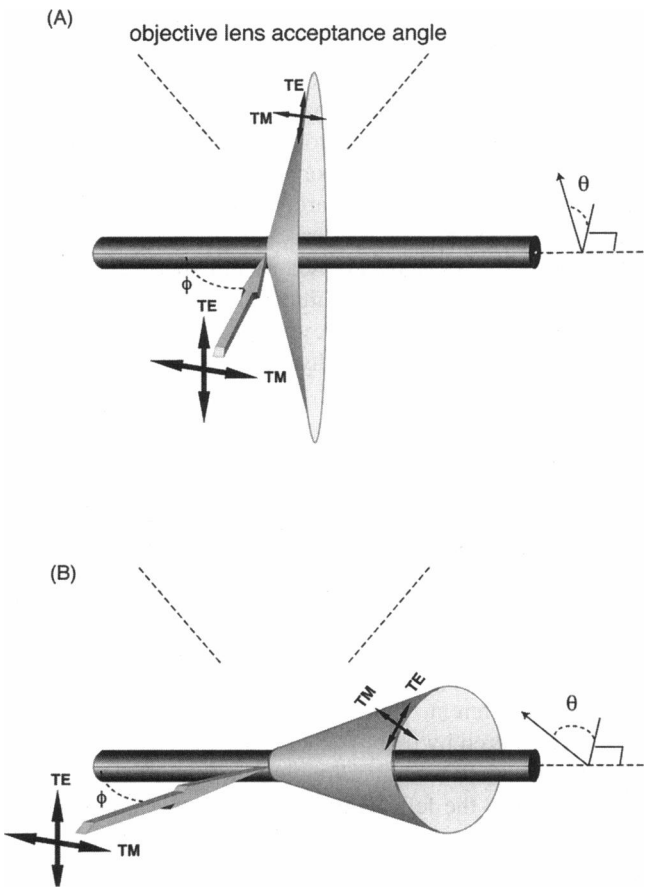

FIGURE 2 The geometry of light scattering by a thin cylinder. The distribution of the scattered light depends on the angle of the illumination relative to the cylinder axis (ϕ). At perpendicular incidence, the scattered light is confined to the incident plane. As the angle of incidence is changed away from 90°, the scattering plane collapses into a cone, the apex angle of which is twice the angle of incidence. Directions around this conical surface are indicated by the angle of observation, θ, as shown in the figure. The dashed lines above the cylinder mark the limiting aperture of the objective lens that is used to form the image of the cylinder (drawn here for an upright microscope, but note that our experimental setup, shown in Fig. 1, actually used an inverted microscope). Light from the cylinder in *A* is scattered into the objective, but from the cylinder in *B* the light is scattered at an angle that cannot be collected by this lens. Thus the cylinder in *B* would be invisible in the microscope at this orientation relative to the incident light. The two possible polarization states of the incident and scattered beams are illustrated by the arrows indicating electric vector oscillation planes.

RESULTS

Fig. 1 shows the optical arrangement for our measurements. Light from a mercury arc lamp is directed with steering mirrors through a rotatable polarizer and then into one side of a glass cube. The sample was mounted in aqueous buffer between two glass coverslips on the rotating stage of an inverted microscope. A very thin layer of immersion oil with refractive index matching that of the glass was used to connect the top surface of the upper coverslip to the bottom surface of the glass cube. We chose the angle of entry of the light into the glass cube so that total internal reflection of the incoming light occurred at the interface between the upper coverslip and the water, generating an evanescent wave that could interact with a sample located very close to the glass-water interface (Axelrod, 1981; Ambrose, 1956, 1961).

Light scattered from the sample was observed through an objective lens coupled to the lower coverslip with a drop of immersion oil, and recorded with a CCD camera with on-chip integration. A rotatable analyzer was positioned between the objective and the eyepiece or camera. We recorded images of the specimen as it was rotated through 180° in 4° increments, using four different polarizer-analyzer combinations. The two settings of the polarizer were such that the plane of oscillation of the incoming light electric vector was either perpendicular or parallel to the glass-water interface. Using the notation of Bohren and Huffman (1983), these two cases correspond to the TE (transverse electric vector) and TM (transverse magnetic vector) modes of illumination, respectively (see Fig. 2). For each of these two modes of illumination, we observed the

resultant scattering through analyzer orientations that selected light oscillating parallel to the X (horizontal) or the Y (vertical) axes of our image. Stated in terms of the sample cylindrical polar coordinate system, these two analyzer orientations select electric vector oscillations parallel to an axoneme for which $\phi = 0°$ or 90°, respectively. The four polarizer-analyzer settings are denoted by TEX, TEY, TMX, and TMY.

We used the axonemes of sea urchin sperm flagella as a convenient source of large numbers of identical, well-characterized, long, straight, thin cylindrical objects. From electron microscopy of frozen hydrated specimens (Murray, 1986), the average diameter of an axoneme in water is known to be 260 nm.

Fig. 3 shows light microscopic images of a field of axonemes viewed with different combinations of incident and scattered light polarization states. An electron micrograph of a cross section of an axoneme is also shown for reference. The sample contains axonemes distributed randomly in all possible orientations, as shown in the top right image of Fig. 3. Exactly the same field of view is included in all five of the light micrographs of Fig. 3, but the images look quite different. Clearly, the intensity and polarization of light scattered by these particles depend strongly on their orientation relative to the direction of illumination (illumination is from the left parallel to the x axis in all images). These intensity variations are an intrinsic property of thin cylinders (Bohren and Huffman, 1983; Van de Hulst, 1957; Kerker, 1969).

Although we have used evanescent wave illumination, the same phenomenon is readily observed with axonemes when using dark-field illumination, or indeed, with light scattering from any thin cylinder when using directional illumination of any kind. (A convincing laboratory demonstration is easily set up using a laser pointer and a thin wire.) We used evanescent wave illumination in these experiments because this makes it very simple to determine the exact angle of illumination for every axoneme. The intensity of the evanescent wave decays exponentially with perpendicular distance away from the glass-water interface. In our experimental setup, the illumination intensity is expected to decay by $1/e$ in a distance of approximately 150 nm (Axelrod, 1989), thus ensuring that all of the particles we observe are very close to the glass-water interface and therefore perpendicular to the optical axis of the microscope. This greatly simplifies our measurements and analysis, because their orientation with respect to the incident light is then specified by a single angle, a rotation around the optic axis. Changes in the angle of illumination are thus exactly equal to the changes in rotation angle of the microscope stage.

The intensity of light scattered by individual axonemes changes dramatically as they are rotated through different orientations relative to the direction of illumination. Fig. 4 shows images, and Fig. 6 shows quantitative measurements, of scattered intensity as a function of illumination angle at a N.A. of 0.8. Similar data were also obtained at a N.A. of 1.04. The data of Fig. 6 were obtained by repeated measurements on the same axoneme, with the rotating stage turned to various positions while the incoming light remained fixed. Under the TMY or TEX conditions, axonemes that are nearly perpendicular to the incident light are easily seen. With TMX or TEY, however, only axonemes at an angle of 90 ± 20–30° are seen.

A mercury arc lamp was used for illumination in the experiments of Figs. 3, 4, and 6. We also carried out the same experiments using an argon ion laser as the light source. The results were the same with the laser and the arc lamp, but quantitation is less satisfactory with the laser, because of the intensity variations across the field of view caused by interference fringes.

Theoretical results

As a first approximation, we represent the axoneme by an infinitely long, homogeneous solid cylinder (see Fig. 3 for a cross-sectional view of the real structure). The starting point for our calculation of the appearance of this model structure in a polarizing microscope is Maxwell's equations. Solutions to Maxwell's equations for an infinite dielectric cylinder in an electromagnetic field have been known for some time (Bohren and Huffman, 1983; Van de Hulst, 1957; Kerker, 1969; Wait, 1955; see also corrections in Wait, 1965; Farone and Querfeld, 1966). The form of the solution presented by Bohren and Huffman (1983) is convenient for computation and for introducing modifications appropriate to microscopic observation (approximations to the exact solution have been employed in a number of areas; for a review of some applications in polymer chemistry, see Stein et al., 1966). The variables that occur in those equations are as follows. An infinitely long cylinder of radius R and refractive index N_2 is immersed in a medium of refractive index N_1 and illuminated by light propagating at an angle ϕ with respect to its axis ($\phi = 90°$ for perpendicular incidence). Taking into account the polarization state of the illumination, we distinguish two cases. If the plane of the electric vector oscillation is parallel to the plane containing both the particle axis and the direction of propagation of the incident light, then the incident illumination is denoted as TM (transverse magnetic vector) mode. The alternative TE (transverse electric vector) mode indicates light with electric vector oscillating perpendicular to the plane containing both the cylinder axis and the illumination direction (see Fig. 2). For convenience in the equations to follow, we will distinguish these two polarization states by subscript 1 for TM mode and 2 for TE mode illumination.

The geometry of light scattering by cylinders is quite remarkable. The scattered light propagates away from the cylinder on the surface of a cone that has the cylinder as its axis. This surprising phenomenon is the consequence of having a linear arrangement of point scatterers: the phase relationship between waves scattered from neighboring points ensures that they add constructively only on the

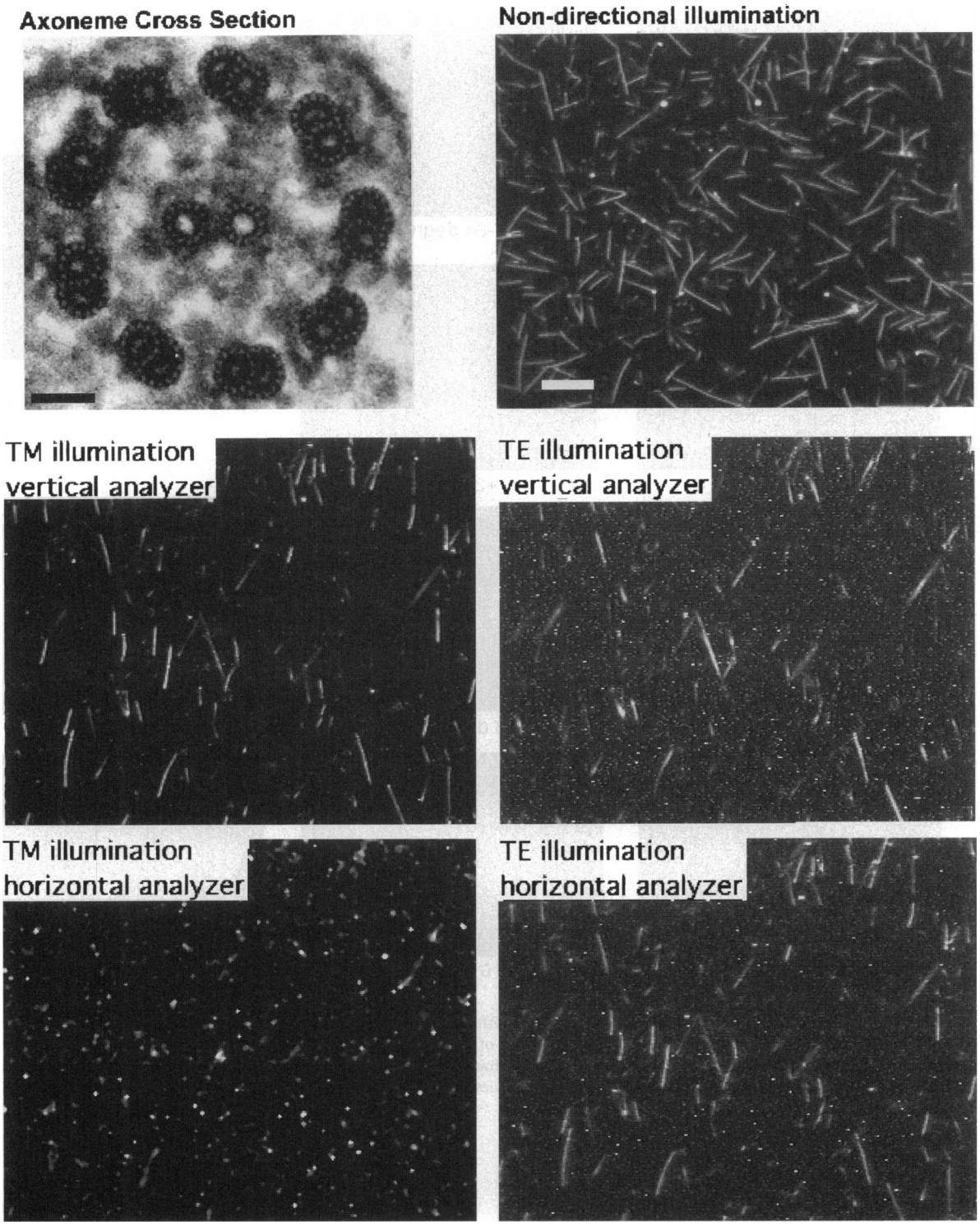

FIGURE 3 Images of flagellar axonemes. At the top left is an electron micrograph of a cross section of a flagellar axoneme. At the top right is an image of a field of flagellar axonemes viewed with nondirectional illumination. Axonemes at all orientations are clearly seen. The middle and bottom rows show four images of the same field of view that was included in the top right image, but using directional illumination with four different polarizer-analyzer combinations (*middle row:* TMY, TEY; *bottom row:* TMX, TEX). The direction of propagation of the incident light is from the left (i.e., from $-X$ to $+X$) in the latter four images. Notice that each polarizer-analyzer combination selects for a different range of orientations. The lower four images were integrated for 25, 300, 500, and 150 frames, respectively, to compensate for the difference in relative intensity with these different settings. The TMX image (*bottom left*) has been noise-filtered and contrast enhanced to show the weakly visible axonemes. Scale bars: top left, 50 nm; top right, 10 μm. The middle and bottom rows are the same magnification as the top right image.

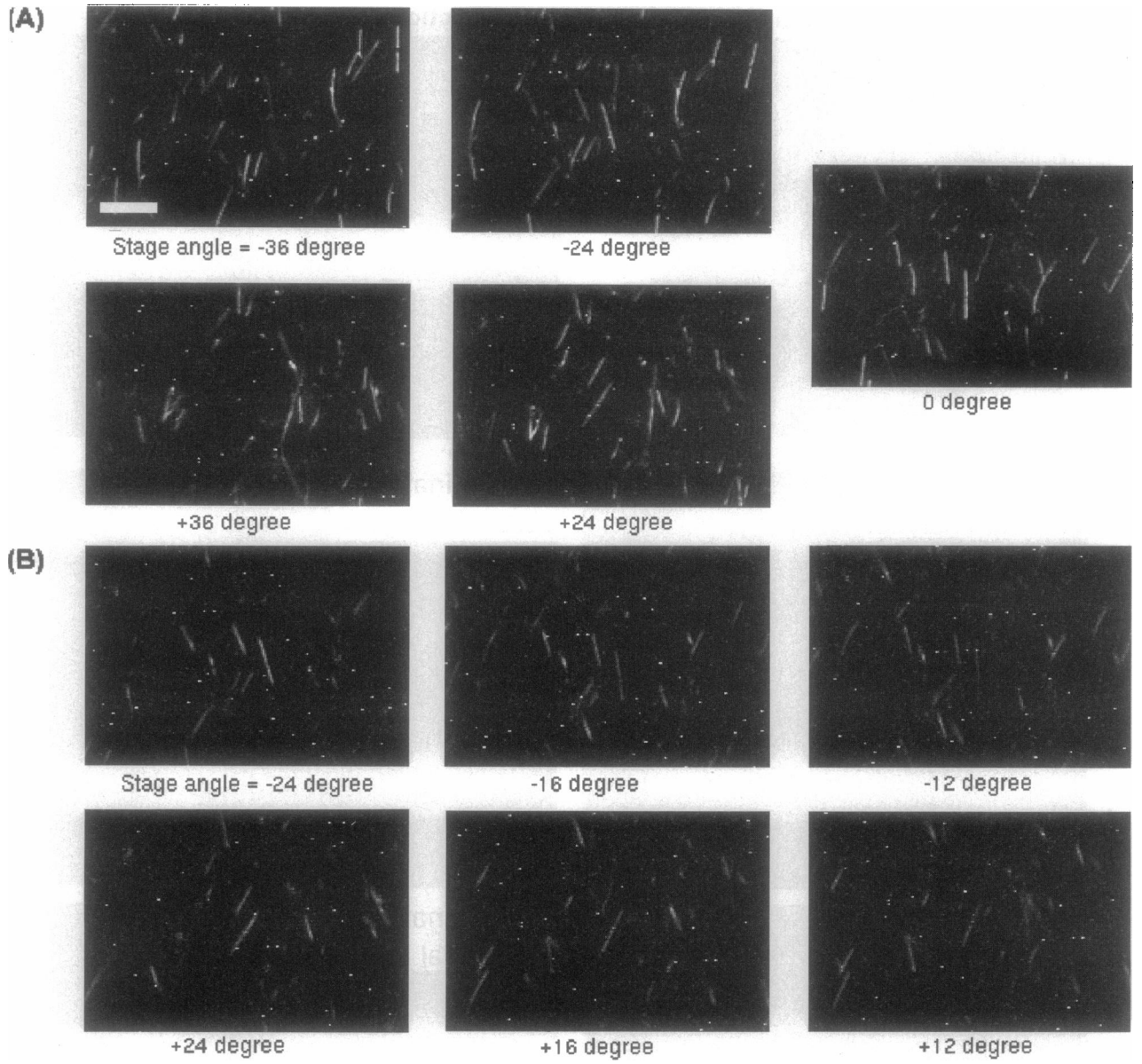

FIGURE 4 Changes in images of axonemes with stage rotation. Two different illumination modes (polarizer settings) with the analyzer vertical are shown. (*A*) The illumination was polarized parallel to the vertical direction of the image (TMY). The same field of view is shown with the rotating stage set to 0° or rotated by ±24° or ±36°. The images were integrated for 25 frames. (*B*) The illumination was polarized perpendicular to the sample plane (TEY), and each image was integrated for 300 frames. The same field of view as in *A* is shown at stage rotations of ±12°, ±16°, and ±24°. Scale bar: 10 μm.

surface of this cone (see, e.g., Kerker, 1969). The included angle of the cone is just twice the angle between the illumination direction and the cylinder (see Fig. 2). The direction of scatter around this conical surface is denoted by angle θ, with $\theta = 0°$ defined as the forward scatter direction (i.e., the direction of the unscattered beam). For the special case of illumination perpendicular to the cylinder ($\phi = 90°$), the scattered light lies entirely in the plane perpendicular to the cylinder axis that also contains the direction of illumination. For this special case, $\theta = 180°$ corresponds to scatter exactly back along the illumination direction (Fig. 2).

For each of the two polarization states of the illuminating beam, we have to consider two possible polarization components of the scattered beam. The scattered light may be polarized with its electric vector either perpendicular to (TM mode) or tangent to (TE mode) the surface of the cone of propagation. We will distinguish the four possible combinations of illumination plus scattered light polarization states by a two-digit subscript, where the first subscript digit refers to illumination (1 = TM; 2 = TE), and the second digit refers to the scattered light polarization (1 = perpendicular to the cone surface; 2 = tangential to the cone surface). Thus E_{11} refers to the complex amplitude of scat-

tered light with polarization perpendicular to the cone surface that arose from TM mode illumination. It follows from the equations to be given below that $E_{12} = E_{21}$ for all scattering angles, and that both are zero for the special case of perpendicular illumination.

The equations relating the amplitude of scattered light to ϕ, θ, distance r from the cylinder, and illumination amplitude E_1 or E_2 (Bohren and Huffman, 1983; Kerker, 1969) are

$$E_{11}(\phi, \theta, r) = \left(\frac{\lambda}{rN_1\pi^2\sin\phi}\right)^{1/2}\left[b_0^{\mathrm{I}} + 2\sum_{n=1}^{\infty} b_n^{\mathrm{I}}\cos(n\theta)\right]E_1$$

$$E_{22}(\phi, \theta, r) = \left(\frac{\lambda}{rN_1\pi^2\sin\phi}\right)^{1/2}\left[a_0^{\mathrm{II}} + 2\sum_{n=1}^{\infty} a_n^{\mathrm{II}}\cos(n\theta)\right]E_2$$

$$E_{12}(\phi, \theta, r) = \left(\frac{\lambda}{rN_1\pi^2\sin\phi}\right)^{1/2}\left[-2i\sum_{n=1}^{\infty} b_n^{\mathrm{II}}\sin(n\theta)\right]E_1$$

$$E_{21}(\phi, \theta, r) = \left(\frac{\lambda}{rN_1\pi^2\sin\phi}\right)^{1/2}\left[-2i\sum_{n=1}^{\infty} a_n^{\mathrm{I}}\sin(n\theta)\right]E_2$$

In these equations r is the distance from a point on the cylinder to the point of observation on the surface of the scattering cone. The precise value chosen for r does not really matter. The choice determines the absolute intensities, which are not easily measured in our experiment (see Discussion), but has no effect on the relative intensities of the different polarization components. We used a value that approximated the distance from the cylinder to the entrance aperture of the objective lens. The coefficients a and b are obtained by requiring that the scattering from the cylinder be a solution of the scalar wave equation expressed in cylindrical polar coordinates, and in addition that the tangential components of the electric and magnetic fields be continuous at the boundary between the surface of the cylinder and the surrounding medium (Bohren and Huffman, 1983; Kerker, 1969). The solutions are combinations of Bessel functions and their derivatives as shown below:

$$a_n^{\mathrm{I}} = \frac{C_nV_n - B_nD_n}{W_nV_n + iD_n^2} \qquad a_n^{\mathrm{II}} = \frac{A_nV_n - iC_nD_n}{W_nV_n + iD_n^2}$$

$$b_n^{\mathrm{I}} = \frac{B_nW_n + iC_nD_n}{W_nV_n + iD_n^2} \qquad b_n^{\mathrm{II}} = \frac{-i(C_nW_n + A_nD_n)}{W_nV_n + iD_n^2}$$

$$A_n = i\alpha[\alpha J_n'(\beta)J_n(\alpha) - \beta J_n(\beta)J_n'(\alpha)]$$

$$B_n = \alpha\left[\alpha\left(\frac{N_2}{N_1}\right)^2 J_n'(\beta)J_n(\alpha) - \beta J_n(\beta)J_n'(\alpha)\right]$$

$$C_n = n\beta\left(\frac{\alpha^2}{\beta^2} - 1\right)\cos\phi J_n(\beta)J_n(\alpha)$$

$$D_n = n\beta\left(\frac{\alpha^2}{\beta^2} - 1\right)\cos\phi J_n(\beta)H_n(\alpha)$$

$$V_n = \alpha\left[\alpha\left(\frac{N_2}{N_1}\right)^2 J_n'(\beta)H_n(\alpha) - \beta J_n(\beta)H_n'(\alpha)\right]$$

$$W_n = i\alpha[\beta J_n(\beta)H_n'(\alpha) - \alpha J_n'(\beta)H_n(\alpha)]$$

$$\alpha = \frac{2\pi RN_1\sin\phi}{\lambda} \qquad \beta = \frac{2\pi RN_1}{\lambda}\sqrt{\left(\frac{N_2}{N_1}\right)^2 - \cos^2\phi}$$

$J_n(X)$, $J_n'(X)$: Bessel function of the first kind and its derivative

$$J_n'(X) = \frac{(J_{n-1}(X) - J_{n+1}(X))}{2}$$

$H_n(X)$, $H_n'(X)$: Hankel function and its derivative

$$H_n'(X) = J_n'(X) + \frac{i}{2}(Y_{n-1}(X) - Y_{n+1}(X))$$

$Y_n(X)$: Bessel function of the second kind.

For illustration, the angular distribution of the intensity ($I_n = |E_n|^2$) of the scattered light around the conical surface is shown in Fig. 5 for a few situations typical of the conditions in our experiments.

To apply this theoretical framework to our observations, we need to modify these equations to take into account the effects of finite observing aperture, reflection at the glass-water interface, and orientation of the analyzer. We observe this scattered light through a microscope, which forms an image of the cylinder. The brightness of each point in the image of the cylinder will depend on how strongly the cylinder scatters light and how much of the light scattered from the corresponding point in the specimen is collected by the objective lens. We compute the relative brightness of particles illuminated from different angles as the square of the amplitude function integrated around the surface of the cone over the entire range of scattering angles that can be collected by our objective lens. That is, we need the integral:

$$I(\phi, r = r_1) = \left|\int_{\theta_{\min}}^{\theta_{\max}} E(\phi, \theta, r = r_1)\mathrm{d}\theta\right|^2$$

The finite aperture of the objective lens limits the range of scattering angles that can be observed. The effect of finite aperture is thus to gradually reduce the fraction of scattered light collected from its maximum value (when $\phi = 90°$) to zero outside the range defined by $|90° - \phi| \leq \sin^{-1}$ [N.A./1.33]. Particles oriented such that ϕ is beyond these limiting values are thus invisible. For a given N.A. and cylinder orientation ϕ, the range of scattering angles θ that

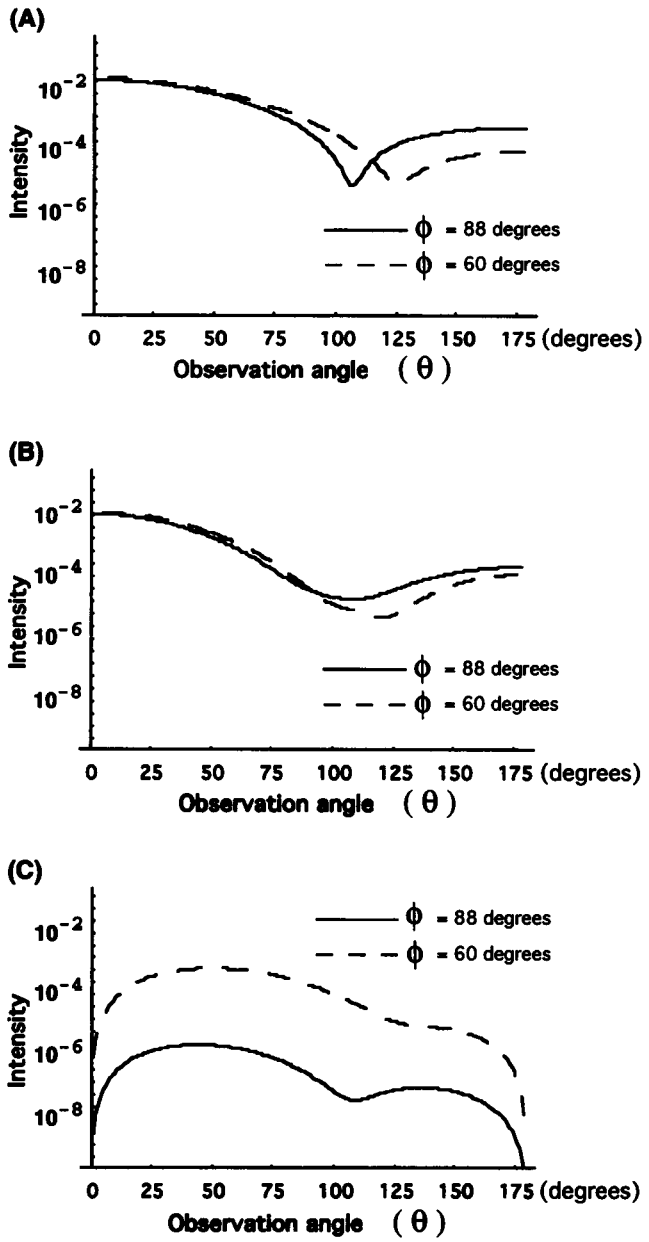

FIGURE 5 Intensity distribution around the cone of scattered light. Plots of the calculated intensity distributions (on a logarithmic scale) around the cone of scattering light are shown for each polarization condition. (*a*) I_{11}; (*b*) I_{22}; (*c*) I_{12}, which is equal to I_{21}. Two angles of incidence ($\phi = 88°$ and 60°) are shown for each condition. The incident light has intensity of 1.0. Only part of this scattered light could be captured by an objective lens, depending on its numerical aperture.

is collected by the lens is

$$\theta_{\text{min, max}} = 90° \pm \cos^{-1}\{\cos[(\sin^{-1}(\text{N.A.}/1.33)]/\sin\phi)\}.$$

However, within this limiting range, the transmittance varies with angle. A complete statement of this variation in transmittance with entrance angle is provided by the optical transfer function (OTF) of the objective lens. For the objective lens used here, we determined the OTF empirically by using a resolution test slide (Young, 1989).

Light scattered from the cylinder propagates through the aqueous medium and strikes the lower coverslip at an angle that depends on the direction of scattering. Part of this light will be reflected, the value depending on the angle of incidence and direction of polarization. The fractions of the intensities that are transmitted (i.e., not reflected) for scattered light with electric vector oscillating perpendicular and parallel to the glass-water interface, t_1 and t_2, respectively, are

$$t_1 = \begin{cases} 1.0, & \varphi_i + \varphi_r = \pi/2 \\ 1.0 - \left(\dfrac{N_{\text{glass}} - N_{\text{water}}}{N_{\text{glass}} + N_{\text{water}}}\right)^2, & \varphi, \varphi_r = 0 \\ 1.0 - [\tan(\varphi_i - \varphi_r)/\tan(\varphi_i + \varphi_r)]^2, & \text{otherwise} \end{cases}$$

$$t_2 = \begin{cases} 1.0 - \left(\dfrac{N_{\text{glass}} - N_{\text{water}}}{N_{\text{glass}} + N_{\text{water}}}\right)^2, & \varphi_i, \varphi_r = 0 \\ 1.0 - [\sin(\varphi_i - \varphi_r)/\sin(\varphi_i + \varphi_r)]^2, & \text{otherwise} \end{cases}$$

$$\varphi_i = \cos^{-1}(\sin\phi \sin\theta) \quad \text{angle of incidence}$$

$$\varphi_r = \sin^{-1}\left(\frac{N_{\text{water}}}{N_{\text{glass}}} \sin\varphi_i\right) \quad \text{angle of refraction.}$$

To account for the effect of the analyzer, it is useful to represent the scattered light polarization as the two-dimensional unit vector obtained by projection of the three-dimensional vector onto the plane of the analyzer. The analyzer orientation is also specified as a two-dimensional unit vector, in our case a vector parallel to either the *X* or the *Y* axis. The fractional transmittance of the scattered light is then calculated as its dot product with the analyzer vector. The fractions of the scattered light intensity passed by the analyzer for the four combinations of analyzer and polarizer orientations are

$$t_{\text{TMX}} = \frac{(\cos\phi \sin\phi \cos\theta - \cos\phi \sin\phi)^2}{(\cos\phi \cos\theta)^2 + \sin^2\phi}$$

$$t_{\text{TMY}} = \frac{(\cos^2\phi \cos\theta + \sin^2\phi)^2}{(\cos\phi \cos\theta)^2 + \sin^2\phi}$$

$$t_{\text{TEX}} = \sin^2\phi$$

$$t_{\text{TEY}} = \cos^2\phi$$

Numerical integration of the $E(\phi, \theta)$ equations, modified as described above to correspond to observation through the glass-water interface, objective lens, and analyzer, was carried out for the range of values of ϕ (in 1° increments) that could be observed with the numerical aperture used in our experimental measurements (0.80 or 1.04). The curves shown in Fig. 6 are for N.A. 0.8, axoneme radius of 130 nm, and refractive index 1.512. (The latter value was taken from experimental measurements of refractive index for another object, the mitotic spindle, composed of microtubules (Sato et al., 1975).) In all cases, both the experimental data and

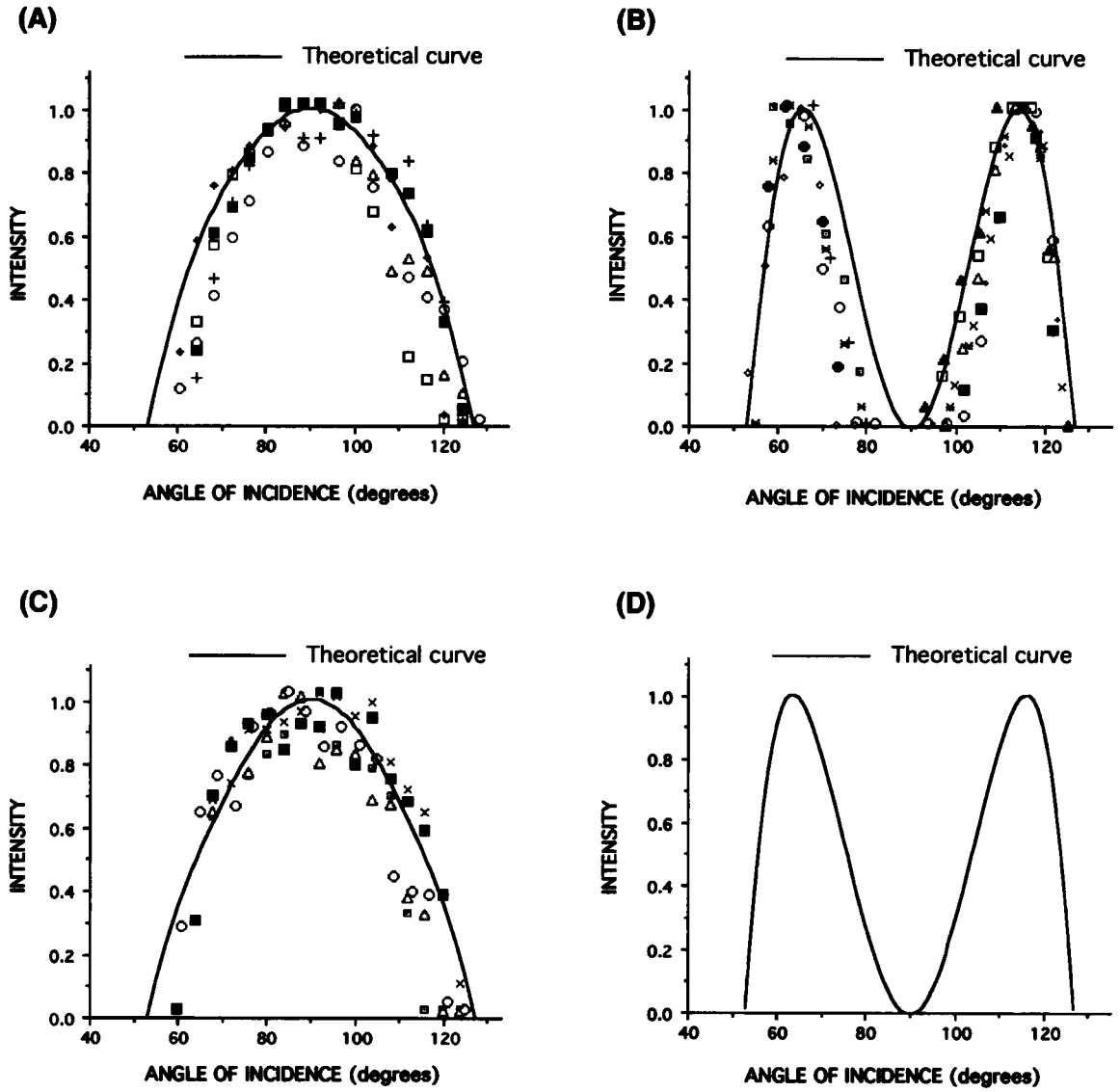

FIGURE 6 Calculated and measured intensity in the microscope as a function of orientation. Comparison of calculated (*solid lines*) and observed (*symbols*) microscopic light scattering intensity as a function of illumination angle for different polarizer-analyzer combinations. (*A*, TMY; *B*,TEY; *C*, TEX; *D*, TMX) Each type of symbol corresponds to repeated measurements made on the same axoneme at different orientations. The data have been normalized so that the maximum intensity in each condition is 1.0. Our calculations satisfactorily account for the angular dependence of the light scattering. However, the calculations for a homogeneous solid cylinder predict that the intensity of the scattering for TMX should be of approximately the same magnitude as for TEY, and should have a similar angular dependence. In fact (see Fig. 3) the TMX scattering from axonemes is weaker than TEY. Because the TMX signal is comparable to the readout noise of our video-rate CCD camera, the intensity measurements for this condition are inaccurate; only the calculated shape of the intensity versus orientation curve is shown for this condition .

calculated curves have been normalized to make the maximum intensity value 1.0. Similar shapes of the curves and agreement between data and calculation were obtained at N.A. 1.04. The curves are calculated for a particle on the optic axis (i.e., in the center of the field of view of the objective). However, most of the axonemes used for measurement were displaced from the center of the field, and in some cases were near the periphery. Thus the effective N.A. of the objective is slightly lower for some of the axonemes included in our measurements, as can be seen in Fig. 6. For example, in Fig. 6 *A*, the filled squares fit the theoretical curve for N.A. 0.8 quite closely, whereas the open circles would fit better with a N.A. of approximately 0.7.

DISCUSSION

The image of thin rods formed by a light microscope is strongly dependent on the direction of propagation and the polarization state of the incident light. Measuring the intensity of light scattered from axonemes of sea urchin sperm flagella, we observed large changes as the axoneme is

rotated through different orientations relative to the direction of illumination. The shape of the intensity versus orientation curves differs markedly for different polarization states of the incident and scattered light. By modeling the axoneme as an infinitely long, homogeneous thin cylinder, we were able to construct equations for the light scattering as a function of orientation of the axoneme and the polarization conditions. Our equations account quite well for the characteristic shapes of the normalized intensity versus orientation curves.

We interpret this agreement between the shapes of the calculated and measured curves as an indication that our formulation of the phenomenon is basically correct. We are not able to compare the absolute intensities in our measurements with theoretical predictions because of uncertainties concerning the intensity of the illumination. We chose to use evanescent wave illumination for these studies because it ensures that all of our scattering particles lie in one plane, which greatly simplifies the problems of defining their orientation relative to the incident light (i.e., a rotation of the stage by a known angle changes the direction of illumination by exactly the same angle). Unfortunately, the disadvantage of this mode of illumination is that it is difficult to determine its intensity.

Axelrod (1989) gives formulae for calculating the relative intensity of the evanescent waves generated with different polarization and angles of the totally internally reflected beam. Using those formulae, and taking into account the partial polarization expected to occur at the glass-air interface on the side of the glass cube, the estimated relative intensities of the evanescent waves with polarization in the x, y, and z directions (see Fig. 1) in our experimental setup are 0.08, 1.23, and 1.45 times the intensity of the original beam from the mercury arc lamp, respectively. An x-polarized component can be produced only with p-polarized (i.e., our TE mode) illumination, and it becomes quite weak if the angle of incidence at the glass-water interface deviates by only a few degrees from the critical angle for total internal reflection (Axelrod, 1989). Presumably for this reason, the actual relative intensity of the x-polarized component in our experiments was much smaller than our estimate. We can be confident that it was very weak, because the light scattered in the forward direction (i.e., $\theta = 0$) from axonemes interacting with an x-polarized component of illumination would always be directed along the optic axis, regardless of the orientation of the axoneme. Therefore, some scattered light from every axoneme would always enter the objective lens, no matter how the stage was rotated (i.e., it could never be completely invisible). In fact, however, we find that each axoneme can be made invisible by rotating the stage to an appropriate orientation. Therefore, we omitted the x-polarized component in our calculations, because the experimental data show that it was too weak to contribute significantly to the observed scattering.

The maximum intensity predicted by our calculations for optimally oriented axonemes (i.e., those with orientation corresponding to the peaks in the intensity versus orientation curves of Fig. 6) under the different polarization conditions are 0.60, 0.16, 0.13, and 0.20 for TMY, TMX, TEY, and TEX, respectively. Taking TEX as the base, the expected relative maximum intensities are in the ratio 3.1: 0.85:0.64:1.00. The relative intensities actually observed are 5.8:0.06:0.39:1.00. Thus for TE mode illumination, the relative intensity observed with the two possible analyzer settings (0.39:1.00) is not far from our calculations (0.64: 1.00). For TM illumination, the agreement is not very good; the calculations predict a 3.6-fold difference in intensity between X and Y analyzer settings (0.85:3.1), whereas we observe a 100-fold difference (0.06:5.8).

One trivial explanation for this discrepancy might be that there is a "bug" in our computer programs, or an error in the equations themselves. We think both of these possibilities are quite unlikely, for the following reasons. First, the starting point for our analysis, the solutions to Maxwell's equations for an infinite cylinder, have been extensively checked against experimental data for the case of silica fibers in air, and found to be extraordinarily accurate (Farone and Querfeld, 1966; Farone and Kerker, 1966; Kerker et al., 1966). We used the corresponding part of our program to compute numerical values to compare with the published silica fiber data and found them to be in perfect agreement. Second, the characteristic shape of the intensity versus orientation curves is well predicted by our calculations. Third, the calculated relative intensities for TE mode illumination match the data well, whereas TM does not. The difference between these two situations in the computer program is very small; most parts of the calculations are common to both situations. The analyzer-specific parts of the computer program have been checked in isolation from the remainder and proved to be correct. Fourth, at several intermediate points of the calculation we carried out internal consistency checks, which were in all conditions accurately satisfied. Fifth, for certain special conditions (e.g., very small N.A. observation of particles illuminated at perpendicular incidence) the intensity and polarization state of the scattering can be deduced from simple physical considerations without any calculation (e.g., see Bohren and Huffman, 1983), and in those situations the calculated values are always correct.

A second possible source of the discrepancy might be some unrecognized consequence of using evanescent wave illumination. However, we emphasize again that the phenomena we observed are readily reproduced, although more difficult to quantitate, with conventional dark-field illumination. In particular, we measured the approximate maximum relative intensities in fields of randomly oriented axonemes using directional dark-field illumination for the various polarizer-analyzer settings. The values were 5.8: 0.09:0.95:1.00, similar to the more accurately measured ratios obtained with evanescent wave illumination. Thus the character of the illumination is not likely the source of the discrepancy. Similarly, our observations were essentially unchanged by using different microscopes or different objective lenses.

A much more interesting reason, and the most likely one, for the discrepancy between our calculations and our measurements is that our simple model of the axonemes as a homogeneous solid cylinder is inadequate. (In this connection it is worth noting that the less-than-infinite length of our axonemes is not likely to be a source of error. The effects of the ends of the cylinder become insignificant for thin cylinders with a length of more than about 10 times their diameter (Bohren and Huffman, 1983).) As shown in the electron micrograph of Fig. 3, the axoneme is not homogeneous, but instead has a complex internal structure. Nevertheless, the entire diameter of the axoneme spans barely one-half of one wavelength of our illumination. To convert its cross section to that of a homogeneous cylinder, one need merely fill in spaces of the order of one-fifth of the wavelength. Axially, the axoneme is periodic with a repeat length of about 100 nm (Murray, 1986), again about one-fifth of the wavelength. Thus, to a resolution of better than one-half of the wavelength, the axoneme is a homogeneous cylinder. For this reason, our first intuition was that the axoneme is so small that the details of its internal structure would be irrelevant. However, this is almost certainly not the case, to our initial surprise. For instance, the angular distribution of scattered light differs quite markedly between cylinders with diameters of 0.012 μm and 0.025 μm ($\lambda/20$ versus $\lambda/40$)! Even at these very small dimensions, differences in structure affect the scattering. Therefore, it is clear that our simplified model of the axoneme as a homogeneous solid cylinder must be inadequate at some level.

There are both theoretical and experimental grounds for expecting that the differences between our idealized model and the real structure of the axoneme would be manifested as discrepancies in the relative intensities of different polarization components of the scattered light. First, theoretical analysis of two concentric infinite cylinders with different dielectric constants has been carried out (Farone and Querfeld, 1966). The effect of converting a homogeneous cylinder into two concentric cylinders (i.e., introducing a radial inhomogeneity) is said to resemble the effect of changing the diameter of the single cylinder (Kerker, 1969). From our own calculations, it is clear that a change in diameter of the model substantially changes the relative intensity of the different polarization components (however, no physically reasonable value for the diameter of our model mimics the observed relative intensities). Second, measurements of the light scattered from suspensions of rod-shaped bacteria have revealed that the relative strengths of some of the polarization components (specific elements of the Mueller matrix) are quite sensitive to the size and shape distribution in the culture of bacteria (Bronk et al., 1995).

Assume for the moment that the mismatch between the axoneme and our idealized homogeneous solid cylinder is indeed the cause of the error in the calculated relative intensities of the TMY and TMX polarization states. The implications of this discrepancy are quite remarkable. The sizes of the structural features that differentiate the axoneme from a homogeneous solid cylinder are a fraction of the wavelength of light. In spite of this, the discrepancies in the intensity ratios approach 30-fold. Thus the ratio of the intensity of these two polarization states may be an exquisitely sensitive probe for structural features of filamentous objects on a scale generally considered far too small for exploration with the light microscope.

A fully analytical calculation is not possible for a model incorporating the actual structure of the axoneme because solutions to Maxwell's equations are possible only for very simple geometry. Quite successful use has been made of a semianalytical approach for other shapes for which a solution of Maxwell's equations is not possible (Draine and Flatau, 1994). This "coupled dipole approximation" is in principle applicable to scattering by any shape, but in practice is limited by the lengthy computations required. At present, the axoneme is unfortunately somewhat beyond the limit of feasible calculation by the couple dipole approximation (several months of workstation class CPU time (Draine and Flatau, 1994)).

One further limitation of the simple model we have used for the present calculations is the assumption of completely parallel incident light. In fact, the beam from our mercury arc lamp diverged by approximately 2°. To include the effect of a finite N.A. of the illumination system, we simply have to integrate over the range of illumination angles, which lengthens the calculation but does not introduce any new complexity. This modification is well worth pursuing, because it opens up the possibility of extending our treatment to normal polarization microscopy. In principle, the way is open to a complete quantitative explanation of the appearance of this type of sample in a typical polarization microscope image.

Most of the birefringence observed in polarization microscope images of fibrous biopolymers such as actin filaments, microtubules, and flagella is a consequence of their highly elongated shape (form birefringence) rather than of any strongly asymmetric polarizability of their constituent protein molecules (intrinsic birefringence). For instance, the intrinsic birefringence of microtubules contributes only about 10% of the total birefringence observed in mitotic spindles (Sato et al., 1975). Equations have been derived by Wiener (1912) and by Bragg and Pippard (1953) for calculating the form birefringence expected of objects of defined shape. However, these equations assume that the measurement of birefringence occurs only on the light scattered in the forward direction. As is easily appreciated from the data and calculations presented here, form birefringence is expected to vary with choice of observation direction. For observations made over a range of angles simultaneously (i.e., a finite aperture optical system), the birefringence should be a function of the particular set of angles included. For this reason apparent birefringence is expected to vary with the N.A. of the illuminating and observing optical components. (The depolarizing effect of high-N.A. lenses is an entirely separate, and in principle correctable, cause of variation of apparent birefringence with N.A. (Inoué and

Hyde, 1957; Inoué, 1951).) The quantitative description of form birefringence, taking into account its aperture dependence, does not seem to have been included in any previous quantitative treatment, but now appears an achievable and worthwhile goal.

SUMMARY

We have presented experimental measurements and theoretical predictions of the orientation dependence of the visibility of long, thin rods in a polarizing light microscope. Our calculations for unidirectional polarized illumination show that long thin rods observed with finite aperture optics 1) are totally invisible when the angle (ϕ) between the object's long axis and incident illumination is outside the range given by $|90 - \phi| \leq \sin^{-1}$ [1.33/64 N.A.$_{obj}$] degrees; and 2) are seen with maximum intensity when $\phi = 90°$ for incident illumination and scattered light polarized either both parallel or both perpendicular to the long axis of the object; whereas 3) two maxima appear at $\phi \cong 90 \pm 25°$ for polarization of the incident illumination parallel to, but the scattered light perpendicular to, the long axis, or vice versa, and 4) in either of these latter conditions, the scattering intensity drops to zero when the illumination is near normal incidence. These counterintuitive predictions are the consequence of 1) the geometry of light scattering from long, thin objects; 2) the relationship between the polarization directions of the incident and scattered light; and 3) the limited acceptance angle of the microscope's objective lens. The predictions were exactly borne out by our experimental measurements of intensity in images of flagellar axonemes. The relative intensities of axonemes viewed with different polarizer-analyzer settings differ from those expected of a homogeneous solid cylinder. These relative intensities provide a sensitive probe for the structures of biological objects with diameters much smaller than the wavelength of light.

We benefited enormously at every stage of this research from the encouragement, suggestions, and profound understanding of microscopy of Drs. Shinya Inoué and Rudolf Oldenbourg at the Marine Biological Laboratory, Woods Hole, MA.

The opportunity to work in that stimulating environment was made possible by the generous support of Nikon, Inc., via the Nikon Summer Fellowship at the Marine Biological Laboratory. JMM also acknowledges the support of grants from the NSF (DCB 9113313) and the National Institutes of Health (R01-GM 50809).

REFERENCES

Ambrose, E. J. 1956. A surface contact microscope for the study of cell movements. *Nature.* 178:1194.

Ambrose, E. J. 1961. The movements of fibrocytes. *Exp. Cell Res. Suppl.* 8:54–73.

Axelrod, D. 1981. Cell-substrate contacts illuminated by total internal reflection fluorescence. *J. Cell Biol.* 89:141–145.

Axelrod, D. 1989. Total internal reflection fluorescence microscopy. *Methods Cell Biol.* 30:245–270.

Bohren, C. F., and D. R. Huffman. 1983. Absorption and Scattering of Light by Small Particles. John Wiley, New York. 193–213.

Bragg, W. L., and A. B. Pippard. 1953. The form birefringence of macromolecules. *Acta Crystallogr. B.* 6:865–867.

Bronk, B. V., S. D. Druger, J. Czégé, and W. P. Van De Merwe. 1995. Measuring diameters of rod-shaped bacteria in vivo with polarized light scattering. *Biophys. J.* 69:1170–1177.

Draine, B. T., and P. J. Flatau. 1994. Discrete-dipole approximation for scattering calculations. *J. Opt. Soc. Am. A.* 11:1491–1499.

Farone, W. A., and M. Kerker. 1966. Light scattering from long submicron glass cylinders at normal incidence. *J. Opt. Soc. Am.* 56:481–487.

Farone, W. A., and C. W. Querfeld. 1966. Electromagnetic scattering from radially inhomogeneous infinite cylinders at oblique incidence. *J. Opt. Soc. Am.* 56:476–480.

Gibbons, B. H. 1982. Reactivation of sperm flagella: properties of microtubule-mediated motility. *Methods Cell Biol.* 25:253–71.

Inoué, S. 1951. Studies on depolarization of light at microscope lens surfaces. I. The origin of stray light by rotation at lens surfaces. *Exp. Cell Res.* 3:199–207.

Inoué, S., and W. L. Hyde. 1957. Studies on depolarization of light at microscope lens surfaces. II. The simultaneous realization of high resolution and high sensitivity with the polarizing microscope. *J. Biophys. Biochem. Cytol.* 3:831–838.

Kerker, M. 1969. The Scattering of Light and Other Electromagnetic Radiation. Academic Press, New York. 255–310.

Kerker, M., D. Cooke, W. A. Farone, and R. A. Jacobsen. 1966. Electromagnetic scattering from an infinite circular cylinder at oblique incidence. I. Radiance functions for $m = 1.46$. *J. Opt. Soc. Am.* 56:487–491.

Murray, J. M. 1986. Electron microscopy of frozen hydrated eukaryotic flagella. *J. Ultrastruct. Mol. Struct. Res.* 95:196–209.

Murray, J. M., and D. Eshel. 1992. Evanescent-wave microscopy: a simple optical configuration. *J. Microsc.* 167:49–62.

Sato, H., G. W. Ellis, and S. Inoué. 1975. Microtubular origin of mitotic spindle form birefringence. Demonstration of the applicability of Wiener's equation. *J. Cell Biol.* 67:501–517.

Stein, R. S., P. Erhardt, J. J. van Aarsten, S. Clough, and M. Rhodes. 1966. Theory of light scattering from oriented and fiber structures. *J. Polym. Sci.* 13C:1–35.

Van de Hulst, H. C. 1957. Light Scattering by Small Particles. John Wiley and Sons, New York.

Wait, J. R. 1955. Scattering of a plane wave from a circular dielectric cylinder at oblique incidence. *Can. J. Phys.* 33:189–195.

Wait, J. R. 1965. The long wavelength limit in scattering from a dielectric cylinder at oblique incidence. *Can. J. Phys.* 43:2212–2215.

Wiener, O. 1912. Die Theorie des Mischkorpers für das Feld der stationaren Stromung. *Abh. Sachs. Ges. Akad. Wiss. Math. Phys.* 32:509–604.

Young, I. T. 1989. Characterizing the imaging transfer function. *Methods Cell Biol.* 30:1–45.